

## Advances in Panel Methods

H. Söding (Institut für Schiffbau, Germany)

### Abstract

In spite of improving computers, a number of inviscid CFD problems still suffer from excessive storage and/or computing time requirements. Examples are detailed pressure distributions on propellers in a wake field, ship wave effects for low Froude numbers, ship encounters in a channel, 3D seakeeping problems and instationary flows which are not time-harmonic. Three measures to reduce the computer requirements for such problems are demonstrated: the multigrid method, panel clustering, and a new higher-order panel method. Further, the 'patch' method is presented which allows more accurate resistance computations without increasing time or unknowns.

### 1. Introduction

Computational fluid dynamics (CFD) supports to an increasing extent model tests. An important field are "wave-resistance" computations, which use almost exclusively Rankine panel methods to analyse local flow details, to optimise local hull shapes (especially the bulbous bow) and to align of shaft brackets etc. [1], [2]. However, the resistance is not predicted with sufficient accuracy, and reliability to substitute model experiments. Ordinary higher-order panels increase accuracy for simple test cases (spheroids, Wigley hulls, etc.), but failed only recently to show consistent improvements for real ships in an investigation at our institute, [3]. For slow ships (tankers, inland water vessels), due to time and storage limitations the free-surface grids are chosen often too coarse to resolve the short waves.

Panel methods gain in importance for manoeuvring calculations, [4], [5]. Due to the usually low speeds involved and the asymmetry of the flow, problems with a sufficiently fine and extended dis-

cretisation are even more severe. Two-ship encounter simulations are generally not tackled using Rankine panel methods due to the large number of unknowns required. Seakeeping computations using Rankine panels for bodies with forward speed were reviewed this year by [6]. Here generally the covered free-surface area is larger than in wave-resistance computations, and the grid spacing should be finer to cover a wide band-width of wave lengths that may appear in one computation.

In summary, various hydrodynamical computations of practical relevance would benefit from techniques that allow to use more panels without increasing storage and CPU time requirements. Multigrid and cluster techniques can serve this purpose. For a fixed discretisation, the accuracy can be significantly improved by the 'patch' method. Also a new higher-order panel technique with numerical integration appears promising. Advantages will be demonstrated here for steady double-body flows and one example of a free-surface flow, but all techniques are suitable for steady and unsteady flows with and without a free-surface.

### 2. Patch Method

The aim of the patch method [7] is to increase the accuracy of pressure forces and velocity averages over a patch on a body surface compared to the usual first-order panel methods, without introducing a finer discretisation or the complexity of higher-order panel methods. For a given discretisation, the computing time of the panel method and the patch method are about the same, and so are the program complexity and the accuracy of velocities at single points.

Consider an arbitrary body in an infinite ideal fluid (double-body flow). The boundary condi-

tion on the hull (body surface) is that no water flows through the hull. The usual approach in boundary element methods discretises the hull into a number of elements (panels). The boundary condition is then exactly enforced at one point, the collocation point, located approximately at the panel center.

In the 'patch' method, on the other hand, the total flow through each surface element (patch), and not just at its center, is made to vanish. Using sources distributed over plane or curved panels would lead to complicated integrations; therefore in the patch method simple point sources are used. They are located within the body near to the patch centres. The distance between patch centre and source point may be chosen as the minimum of the following lengths:

- Square root of patch area;
- 1/3 of the local body breadth;
- 1/2 the radius of longitudinal curvature;
- 1/2 the radius of transverse curvature.

The results are not sensitive to this distance; in many applications simply 1/10 of the patch length is used.

In the panel method, velocity and pressure can be determined on the hull directly only at the panel centres; at other points, interpolation has to be used. Pressure forces are, typically, determined by multiplying the pressure at the panel centre with the panel area. The patch method aims just to improve this force formula. In the patch method, potential and velocity are determined at the patch corners instead of at the patch centre, i.e. at a reasonable distance from all point sources. The potential at the patch corners allows a better approximation of the average velocity within the patch than the value at the panel centre, and combining the potential and the velocity at the patch corners allows to determine an accurate average of the pressure within the patch.

For a body in uniform flow to negative  $x$  direction, the potential is

$$\phi = -Ux + \sum_{i=1}^n \sigma_i G_i. \quad (1)$$

$U$  is the speed of the uniform flow,  $\sigma$  the source strength,  $G$  the potential of a Rankine point source:

$$G = \ln r \quad \text{in 2D, and} \quad G = -1/r \quad \text{in 3D,} \quad (2)$$

where  $r = |\vec{x} - \vec{s}|$  is the distance between field point  $\vec{x}$  and source point  $\vec{s}$ .

Let  $M_i$  be the outflow through a patch induced by a point source of unit strength. Then the zero-flow condition for a patch is

$$-UAn_x + \sum_i \sigma_i M_i = 0. \quad (3)$$

Here  $\vec{n}$  is the outward normal on the hull, index  $x$  (and later  $z$ ) designates the respective component of  $\vec{n}$ , and  $An_x$  is the projection of the patch area on a plane  $x = \text{constant}$  (with appropriate sign); for the 2d case of Fig. 1:  $An_x = y_A - y_B$ .

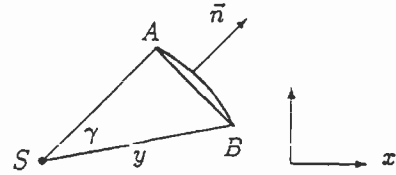


Fig. 1: Patch (from  $A$  to  $B$ ) and source point  $S$

### 2.1 2-d Formulation

The outflow due to the unit source potential  $\ln r$  into all directions is  $2\pi$ . The outflow  $M$  due to the unit source in  $\vec{s}$  passing through the patch in Fig. 1 is thus equal to the angle  $\gamma$  under which the patch is seen from  $\vec{s}$  — both for a straight and a curved patch. If  $\vec{A}$  and  $\vec{B}$  are the vectors from  $S$  to  $A$  and  $B$  respectively,  $\gamma$  is easily determined from the vector and scalar products of  $\vec{A}$  and  $\vec{B}$ :

$$M = \gamma = \arctan \frac{[\vec{B} \times \vec{A}]_z}{\vec{B} \cdot \vec{A}}. \quad (4)$$

From the value of the potential  $\phi$  at the end points  $A$  and  $B$ , the average modulus  $\bar{v}$  of the velocity  $\vec{v}$  is found as  $|\phi_A - \phi_B|/l$ , where  $l$  is the length of the patch. The direction of  $\vec{v}$  is parallel to the contour. The velocity  $\vec{v}$  at the end points, designated here as  $\vec{x}$ , is found as  $\nabla G = (\vec{x} - \vec{s})/r^2$ .

The pressure force on a straight patch is

$$\vec{f} = \vec{n} \int p \, dl = \vec{n} \frac{\rho}{2} \left( U^2 \cdot l - \int v^2 \, dl \right) \quad (5)$$

where  $v$ , the modulus of  $\vec{v}$ , is not constant. To evaluate this expression,  $v$  is approximated by the second-order polynomial giving the known values  $v_A, v_B$  and  $\bar{v}$ :

$$v = v_A + (6\bar{v} - 4v_A - 2v_B)t + 3(v_A + v_B - 2\bar{v})t^2 \quad (6)$$

$t$  is the tangential coordinate directed from  $A$  to  $B$ . From this expression follows the integral in (5):

$$\int v^2 \, dl = l \bar{v}^2 = l \cdot \left( (\bar{v})^2 + \frac{2(v_A - \bar{v})^2 + 2(v_B - \bar{v})^2 - (v_A - \bar{v})(v_B - \bar{v})}{15} \right). \quad (7)$$

As a test case, a symmetric profile with circular nose, parabolic run and a sharp tail, with thickness-chord ratio of 2, was investigated at zero angle of attack. The resistance, which should be zero due to d'Alembert's paradox, is used to indicate the error. (A test body should not be symmetric in  $x$  to avoid cancellation of the discretisation error.) The panel method used for comparison applied straight elements of constant source strength, a collocation scheme and constant pressure over each element.

Table I: Relative resistance (= error) for a foil-shaped profile; comparison of patch method (PTM) with first-order panel method (OPM)

elem. no.	12	24	48	96	192
PTM	17%	13%	5%	1.4%	0.5%
OPM	100%	47%	22%	10%	5%

The patch method proved to be about 5 times more accurate than the panel method, Table I. In other words, only 1/4 of the number of elements of the ordinary panel method sufficed for the patch method to obtain the same force accuracy.

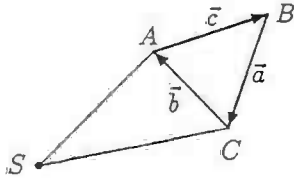


Fig. 2: Source point S and patch ABC

## 2.2 3-d Formulation

The outflow due to the unit source potential  $-1/r$  into all space directions is  $4\pi$ . The outflow due to the unit source in  $S$  passing through the triangular patch in Fig. 2 is thus equal to the space angle  $\gamma$  under which the patch  $ABC$  is seen from  $S$ . Quadrilateral patches are handled by combining two triangles. For straight patch sides, the rules of spherical geometry give  $\gamma$  as the sum of the angles between each pair of planes  $SAB$ ,  $SBC$  and  $SCA$ , minus  $\pi$ ;

$$\alpha = \beta_{SAB,SBC} + \beta_{SBC,SCA} + \beta_{SCA,SAB} - \pi \quad (8)$$

where e.g.

$$\beta_{SAB,SBC} = \arctan \frac{-[(\vec{A} \times \vec{B}) \times (\vec{B} \times \vec{C})] \cdot \vec{B}}{(\vec{A} \times \vec{B}) \cdot (\vec{B} \times \vec{C})|\vec{B}|}$$

Here  $\vec{A}$ ,  $\vec{B}$ ,  $\vec{C}$  are the vectors pointing from the source point  $S$  to the panel corners  $A, B, C$ . Note that a curvature of the patch does not influence the result if the panel edges remain straight. If curved patch sides are approximated by straight lines, the error made in one patch occurs at the neighbouring patch with opposite sign.

$\gamma$  maybe approximated by  $A^*/d^2$  if the distance  $d$  between patch center and source point exceeds a given limit.  $A^*$  is the patch area projected on a plane normal to the direction from the source to the patch center:

$$\vec{d} = \frac{1}{3}(\vec{A} + \vec{B} + \vec{C}) \quad (9)$$

$$A^* = \frac{1}{2}(\vec{a} \times \vec{b}) \cdot \frac{\vec{d}}{d} \quad (10)$$

With known source strengths  $\sigma_i$ , one can determine the potential  $\phi$  and its derivatives  $\nabla\phi$  at all patch corners. From the  $\phi$  values at the corners  $A, B, C$ , the average velocity within the triangle is found as

$$\vec{v} = \nabla\phi = \frac{\phi_A - \phi_C}{\vec{n}_{AB}^2} \vec{n}_{AB} + \frac{\phi_B - \phi_A}{\vec{n}_{AC}^2} \vec{n}_{AC} \quad (11)$$

with

$$\vec{n}_{AB} = \vec{b} - \frac{\vec{c} \cdot \vec{b}}{c^2} \vec{c} \quad \text{and} \quad \vec{n}_{AC} = \vec{c} - \frac{\vec{b} \cdot \vec{c}}{b^2} \vec{b} \quad (12)$$

With known  $\vec{v}$  and corner velocities  $\vec{v}_A$ ,  $\vec{v}_B$ ,  $\vec{v}_C$ , the pressure force on the triangle can be determined from (5) where  $l$  is now the patch area. (7) has the following 3-d equivalent:

$$\int \vec{v}^2 dl = \quad (13)$$

$$l \cdot \left( (\vec{v})^2 + \frac{(\vec{v}_A - \vec{v})^2 + (\vec{v}_B - \vec{v})^2 + (\vec{v}_C - \vec{v})^2}{30} - \frac{(\vec{v}_A - \vec{v})(\vec{v}_B - \vec{v}) + (\vec{v}_B - \vec{v})(\vec{v}_C - \vec{v}) + (\vec{v}_C - \vec{v})(\vec{v}_A - \vec{v})}{90} \right)$$

## 2.3 Test Cases

Test cases concerned a sphere and two ships. The HSVA tanker, used often as a test for RANSE flow codes, has a 'parabolical' bow shape and a much finer afterbody, thus showing the strong asymmetry in  $x$  direction which makes it well-suited to compare the numerically computed resistance in double-body



flow conditions with the correct value of 0. For comparison, Jensen's "sphere method" [12] and a first-order Hess&Smith panel method were applied (Table II). The patch method was more accurate by one order of magnitude for the same discretisation (corresponding roughly to same CPU time and storage requirements for the 3 methods).

Table II. Numerical resistance coefficient  $-2F_x/\rho U^2 S$  by different methods

method	no. of panels/patches	1000 · resistance coefficient
Patch	421	-0.16
Sphere	421	+1.54
Patch	780	+0.03
Sphere	780	+0.20
Hess&Smith	1788	+0.20

Table III shows a comparison of the force on 1/8 of a full sphere in uniform flow. For radius 1 and speed 1, the exact force components on the positive octant are  $f_x = -\pi/64 = 0.04909$  and  $f_y = f_z = 11\pi/128 = 0.26998$ . Here the patch method was compared by Hughes and Bertram [3] with an ordinary higher-order panel method OHM (parabolic in shape, linear in source strength). The patch method is roughly of same accuracy (but much faster) for the longitudinal force, but 3 times more inaccurate for the transverse force. Results of the patch method in Table III refer to a mesh of equilateral triangles; it was found, however, that combining two such triangles to a quadrilateral produced nearly the same error with about half the number of patches.

Table III: Error in force on 1/8 sphere

patch method PTM		
elements	$F_x$ error	$F_y$ error
16	0.006	0.050
64	0.001	0.012
256	0.00005	0.0025
higher-order panel OHM		
elements	$F_x$ error	$F_y$ error
15	0.006	0.017
66	0.002	0.004
231	0.0007	0.0013

Fig. 3 shows the wave resistance coefficient for the Series 60 -  $C_B = 0.6$  hull as a function of Froude number, computed by a non-linear Rankine source / patch method. For the hull boundary condition up to the deformed water surface and for the force integration, the patch method was used,

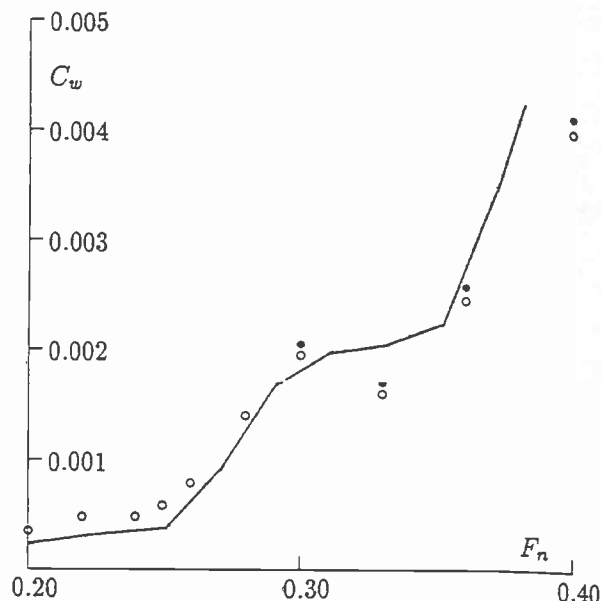


Fig. 3. Wave resistance coefficient of Series 60 ( $C_B = 0.6$ ) model according to experiments ([13], line) and patch method ( $\circ$ ). Symbols  $\bullet$  include interaction with viscous resistance.

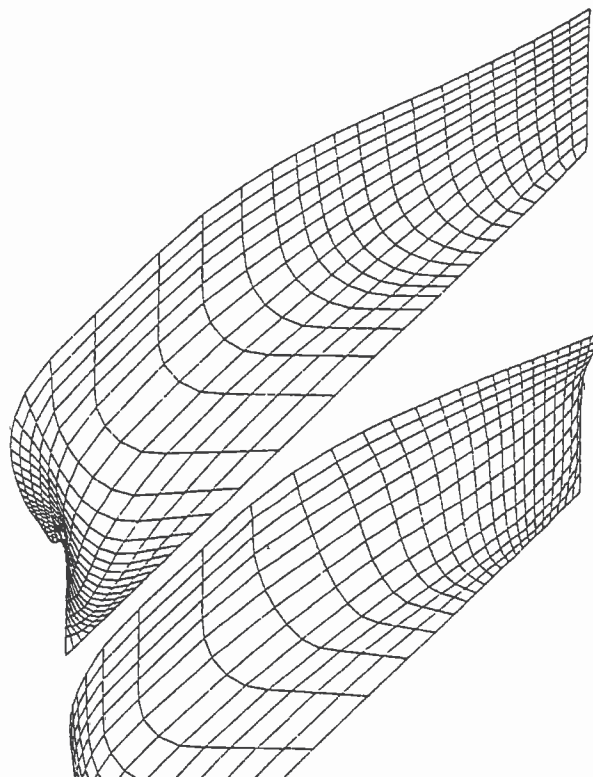


Fig. 4. Patch arrangement on Series 60 hull

whereas the free surface condition was satisfied, as in earlier methods, by point collocation and point sources above the water surface shifted backwards relative to the collocation points. Symbols  $\bullet$  include a rough approximation of the interaction between wave and viscous resistance: the difference between  $\bullet$  and  $\circ$  corresponds to the change of viscous resistance with  $F_n$  estimated to be proportional to the change of wetted surface and to the mean squared non-viscous velocity at the hull surface.

To test the accuracy of the patch method, the hull discretisation shown in Fig. 4 with 37 · 13 patches was modified to have twice the number of patches, either in transverse or in longitudinal direction. The results of the wave resistance were practically the same for all three meshes.

### 3. Cluster and Multigrid Method

#### 3.1 Clustering

In the following only the boundary condition on the body (no flow through the hull) is considered; but clustering and the multigrid technique are even well applicable also for free-surface flow problems.

The discretisation of the hull boundary condition yields a system of linear equations for the unknown source strengths  $\sigma_i$  in (1):

$$K\sigma = g \quad (14)$$

$K$  is the coefficient matrix,  $\sigma$  the vector of source strengths, and  $g$  the vector of the inhomogeneous parts. An element  $k_{ij}$  of  $K$  can be interpreted as flow through a patch  $i$  per time induced by a source of unit strength at point  $\xi_j$ . The elements of  $g$  give the negative flow per time through the patches induced by the uniform flow. Eq. (14) enforces that the superposition of all source flows and the parallel flow add up to zero flow through all patches.

Clustering aims to reduce the computer time and storage requirements for generating the matrix  $K$ , and it simplifies the application of the multigrid method (next chapter); however, clustering and multigrid can be applied also separately. The cluster/multigrid technique is combined here with the patch method, but it could be applied also to ordinary panel methods.

Here, a cluster is a set of 4 by 4 patches of the normal (fine) grid. The 16 patches of each cluster are generated to have similar size and shape, and the surface covered by a cluster should be smooth; if it is not, the cluster should be made smaller.

The scalar equations in (14) referring to a

line of four patches in a cluster are added and subtracted to the following four combined equations:

- 1: + + + +
- 2: + - + -
- 3: + + - -
- 4: + - - +

If the combined equations are satisfied, so are the original ones. The absolute values of coefficients of the combined equations 2, 3, and especially 4 decrease stronger with distance from the main diagonal in  $K$  than those of the original equations and of combination 1.

Correspondingly also the four rows of patches within a cluster are combined to the following 16 combinations of 16 equations:

- 1: + + + + + + + + + + + + + + + +
- 2: + - + - + - + - + - + - + - + - + - +
- 3: + + - - + + - - + + - - + + - - + + - -
- 4: + - - + + - - + - - + - - + - - + - - +
- 5: + + + + - - - - + + + + - - - - + + + +
- 6: + - + - - + - + + - + - + - + - + - +
- 7: + + - - - - + + + + + + - - - - + + - -
- 8: + - - + - + + - + - - + - + - - + - + -
- 9: + + + + + + + + - - - - - - - - - - - -
- 10: + - + - + - + - + - + - + - + - + - + -
- 11: + + - - + + - - - - + + + + - - - - + + - -
- 12: + - - + + - - + - - + - - + - - + - - +
- 13: + + + + - - - - - - - - - - - - + + + +
- 14: + - + - - + - + - + - + - + - + - + -
- 15: + + - - - - + + + + - - + + + + - - - -
- 16: + - - + - + + - - + + - - + + - - + - - +

As the cluster consists of patches of approximately equal size and orientation, for a distant source the influence functions of all combinations will nearly cancel (due to the positive and negative contributions) with the exception of the first combination which adds all influence functions. The purpose of combining the influence of elements within a cluster is, that for large distances between source and patch (resp. collocation point and panel in a conventional panel method) the combined influence functions are so small that they can be neglected. This saves storage space, time for solving the system of equations and - if one can determine a priori which combinations will be neglected - time for computing the influence functions, because only the combined influence functions for all elements of a cluster or for 2 by 2 patch blocks need to be computed.





group are represented.

### 3.2 Multigrid Method

The multigrid method is frequently used for solving differential equations of viscous fluid flow, but it works even better for potential flow problems, i.e. for solving integral equations. The principles of both applications are elaborated in [8]. For panel methods the multigrid technique reduces the time needed to solve the system of linear equations (14) to a negligible fraction of the total computing time.

First, the rows in  $K$  and  $g$  are multiplied by factors such that the elements of  $K$  on the main diagonal are all 1. Then a multigrid solution can be determined as follows: Starting from  $\sigma = \bar{0}$ , a Jacobi iteration step improves  $\sigma$  by smoothing the error in the system of equations on the normal (finest) grid:

$$\bar{\sigma}_l = g_l + (I - K)_l \sigma_l^i \quad (15)$$

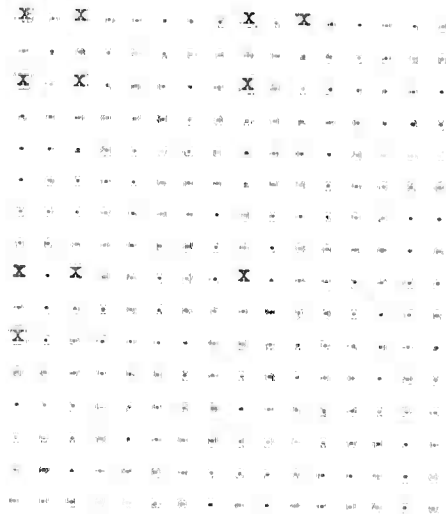
Index  $l$  indicates the grid level:  $l = 3$  denotes the finest grid in the investigated 3-grid method,  $l = 1$  the coarsest grid. Superscripts  $i$  denote the iteration step.  $I$  is the unit matrix,  $\bar{\sigma}$  the improved vector of unknown source strengths.

A straight-forward Jacobi iteration of (15) would take  $\bar{\sigma}_l$  as next iterative solution  $\sigma_l^{i+1}$ . The multigrid method improves convergence by setting

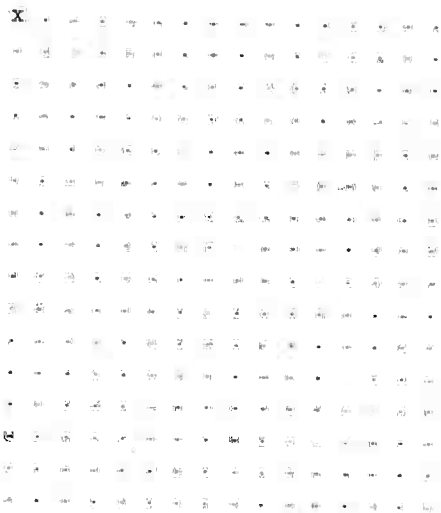
$$\sigma_l^{i+1} = \bar{\sigma}_l - p K_{l-1}^{-1} r \underbrace{(K_l \bar{\sigma}_l - g_l)}_{\mathcal{R}_l} \quad (16)$$

The vector of residuals  $\mathcal{R}_l$  gives the error of all equations. This residual is restricted to a shorter vector, here to 1/4 of the original number of elements, by the restriction operator  $r$  explained later.  $K_{l-1}$  is, correspondingly, a restricted coefficient matrix with 1/4 of the original columns and rows. Multiplication of the residuals with the inverse matrix  $K_{l-1}^{-1}$  yields the necessary corrections to enforce the equations exactly. Because we perform the corrections on a coarser grid, we have to transform them to the original, fine grid by applying the prolongation operator  $p$  (see later). The prolonged corrections added to the approximation  $\bar{\sigma}$  yield the next approximation  $\sigma_l^{i+1}$ . This is again used in (15) and improved by (16) until the residual is decreased by 5 to 6 orders of magnitude.

To determine  $K_2^{-1} r \mathcal{R}_3$  requires to solve a system of linear equations having 1/4 of the original number of unknowns. This system is also solved by applying the multigrid equations (15) and (16), now with  $l = 2$ . There remains a system of 1/16 of the original number of unknowns, which is effectively solved by Gauss' algorithm.



Type 4



Type 5

Fig. 5: Arrangement of non-zero elements ( $z$ ) in five block types

Combined with our clustering technique, the restriction and prolongation operators become extremely simple: For  $l = 3$ , in each block of 16 vector components the restriction operator eliminates 12 components, keeping only the 1st, 3rd, 9th and 11th. That means: In (16) only the flow through 2·2 patch groups is considered, not the flow through single patches. The solution  $K_2^{-1}rR_3$  gives corrections of the source combinations 1, 3, 9, and 11, i.e. corrections of the combined source strength for groups of 2·2 sources. To this end,  $K_2$  is produced from  $K_3$  by keeping in each block of 16·16 elements only those in rows and columns no. 1, 3, 9 and 11. For prolongation, the additional elements, i.e. the corrections of the differences between single source strengths within a block of 2·2 sources, are simply set to zero; these differences are effectively corrected by the Jakobi step (15).

For  $l = 2$ , the restriction operator keeps only the first element of each block of 4 elements, i.e. the combined flux through a 4·4 panel group, and the prolongation operator adds 4 zero elements in each group of 4 components. Matrix  $K_1$  contains the 1st, 5th ... row and column of  $K_2$ .

### 3.3 Test Case

As a test case, the double-body flow around a Wigley hull with 1600 patches (100 clusters) on one ship side was computed. This number of elements is more than necessary for this flow; it is used here only to demonstrate the effect of multigrid and clustering for the typical, larger panel numbers in practical applications. A full coefficient matrix would have required  $1600^2 = 2.56 \cdot 10^6$  coefficients. Clustering reduced this to  $0.35 \cdot 10^6$  (14%) coefficients. The additional storage space is negligible: For each of the 10000 storage blocks, block type and starting address in the coefficient array have to be stored.

On a 12 Mflop computer, the computing time was 73s for determining the coefficient matrix, 2.5s for solving and 33s for determining end results (velocities, pressures, forces). It was necessary to use double precision of the real variables; otherwise the multigrid method did not converge to sufficiently small residuals. A comparison with a coarser discretisation of the Wigley hull involving only 30 clusters (480 patches) showed that the storage requirement was  $\sim n^{1.25}$ , the total computing time  $\sim n^{1.78}$ . Only for systems with more than about 800 elements, the multigrid and clustering approach saved CPU time. However, storage savings are attained already for considerably smaller systems of equations.

## 4. New Higher-Order Panel Method

The purpose of higher-order panels is to increase the accuracy for a given number of unknowns, and to determine spatial derivatives of flow velocities which - for decreasing grid spacing - converge to the correct values. The latter is necessary for sea-keeping calculations with forward speed that linearise around the steady flow potential around the body [9]. The usual higher-order panels following the original work of Hess [10] can compute the necessary velocity derivatives, but they failed to improve accuracy for real ship geometries in [3]. Furthermore they involve quite complicated formulas especially for higher derivatives of the potential.

The new higher-order panel method presented here varies the approach of Kouh and Ho [11]. Both methods are based on a modification of the integrals which give the influence of a source (in my method: and dipole) distribution on the body surface, such that the integrand is non-singular even if the field point is on the body surface, too. This allows to substitute the complicated analytical integration of the singular integrand by a simple numerical scheme.

Differently from [11] and from eq. (1), the 'direct' method is used here. It applies a distribution of sources and dipoles on the body surface and solves directly for the potential at many points on the body surface. Comparisons seemed to indicate that for non-lifting flows (without circulation and without a Kutta condition) both the direct and the indirect method are about even well suited, whereas for lifting flows the direct method is superior in accuracy to the indirect method, which - for lifting flows - uses also sources and line vortices (corresponding to dipole panels).

The well-known equation for the direct (source-dipole) panel method is

$$\begin{aligned} \frac{1}{2}\phi(\bar{x}_0) - \int_{S_b} \phi(\bar{x})\bar{n}(\bar{x})\nabla_x G(\bar{x}, \bar{x}_0) dS(\bar{x}) & \quad (17) \\ = - \int_{S_b} U n_x(\bar{x})G(\bar{x}, \bar{x}_0) dS(\bar{x}) \end{aligned}$$

with the Green function

$$G = -1/(4\pi|\bar{x} - \bar{x}_0|), \quad (18)$$

$\phi$  = disturbance potential,  $\bar{n}$  = unit normal vector on the closed surface  $S_b$ ,  $U$  = ship speed and  $\bar{x}_0$  = a field point on  $S_b$ . The integrals in (17) are desingularised (without moving the singularities into the interior of



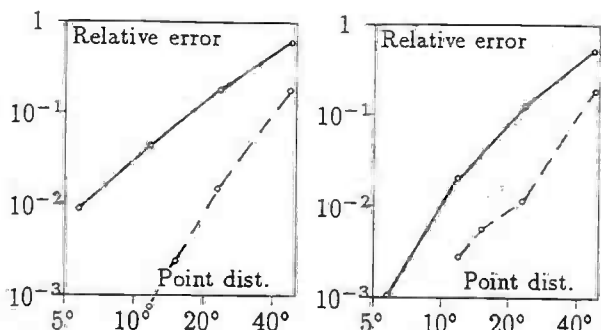


Fig. 6. Relative error of transverse (left) and longitudinal (right) pressure force on 1/8 of a sphere for patch (continuous) and higher-order method (broken line)

the body) in the following equivalent equation:

$$\begin{aligned} \phi(\bar{x}_0) - \int_{S_b} [\phi(\bar{x}) - \phi(\bar{x}_0)] \bar{n}(\bar{x}) \nabla_{\bar{x}} G(\bar{x}, \bar{x}_0) dS(\bar{x}) \\ = - \int_{S_b} \left( U n_x(\bar{x}) - \frac{U n_x(\bar{x}_0) \delta(\bar{x})}{\delta(\bar{x}_0)} \right) G(\bar{x}, \bar{x}_0) dS(\bar{x}) \\ = \frac{U n_x(\bar{x}_0)}{\delta(\bar{x}_0)} \phi_0 \end{aligned} \quad (19)$$

$\phi_0$  is the constant potential generated by the source distribution  $\delta$  in the space surrounded by  $S_b$ , i.e. inside the body.  $\delta$  is the 'eigen potential' following from the homogeneous integral equation

$$\frac{1}{2} \delta(\bar{x}_0) + \int_{S_b} \delta(\bar{x}) \bar{n}(\bar{x}_0) \nabla_{\bar{x}_0} G(\bar{x}, \bar{x}_0) dS(\bar{x}) = 0 \quad (20)$$

Eq. (20) has a solution  $\delta$  which has non-zero values everywhere on  $S_b$ . Eq. (20) is also desingularised:

$$\int_{S_b} [\delta(\bar{x}) \bar{n}(\bar{x}_0) + \delta(\bar{x}_0) \bar{n}(\bar{x})] \nabla_{\bar{x}} G(\bar{x}, \bar{x}_0) dS(\bar{x}) = 0 \quad (21)$$

The nonsingular integrals in (21) and (19) are evaluated by Simpson's rule using 9-knot panels (8 on the circumference, one in the center), to obtain a system of linear algebraic equations for the potential at each knot. Numerical interpolation and differentiation over the panels gives velocities, velocity derivatives, and pressures on  $S_b$ .

For a sphere in uniform flow, Fig. 6 compares relative errors of the pressure force on 1/8 sphere between the higher-order and the patch method. For both methods, the mesh consisted of quadrilaterals bounded by meridians and latitude circles with uniform angular spacing, poles being at the stagnation points. (Results for the patch method given

in Fig. 6 differ somewhat from Table III because there a mesh of nearly uniform, equilateral triangles was used.) The higher-order method is, roughly, 10 times more accurate than the patch method which is again much more accurate than an ordinary first-order panel method. For more complicated bodies, however, the difference is expected to be much smaller. Both the maximum error in  $\phi$  (not shown) and the pressure force (Fig. 6) converge with errors  $\sim h^{3.5}$  to  $h^4$ , where  $h$  is the grid spacing.

## References

1. Bertram, V., "Numerische Schiffshydrodynamik in der Praxis", rep. 545, 1994, Inst. für Schiffbau, Hamburg Univ., Germany
2. Bertram, V.; Jensen, G., "Recent applications of computational fluid dynamics", Ship Techn. Res. 41/3, 1994, pp. 131-134
3. Hughes, M.; Bertram, V., "A higher-order panel method for 3-d free surface flows", rep. 558, 1995, Inst. für Schiffbau, Hamburg Univ., Germany
4. Zou, Z.; Söding, H., "A panel method for lifting potential flows around a yawed ship in shallow water", 20th Symp. on Ship Hydrodyn., 1994, Santa Barbara
5. Zou, Z., "Calculation of the three-dimensional free-surface flow about a yawed ship in shallow water", Ship Techn. Res. 42/1, 1995, pp. 45-52
6. Bertram, V.; Yasukawa, H., "Rankine source methods for seakeeping problems", Proc. Schiffbautechn. Gesellschaft, Springer, Berlin, Heidelberg, New York, Tokyo, 1996
7. Söding, H., "A method for accurate force calculations in potential flow", Ship Techn. Res. 40/3, 1993, pp. 176-186
8. Hackbusch, W., Multi-grid methods and applications, Springer, Berlin, Heidelberg, New York, Tokyo, 1980
9. Bertram, V., "Ship motions by a Rankine source method", Ship Techn. Res. 37/4, 1990, pp. 143-152
10. Hess, J.L., "A higher order panel method for three-dimensional potential flow", NADV-Report, MDC J8519, 1979
11. Kowh, J.S.; Ho, C.H., "A high order panel method based on source distribution and Gaussian quadrature", Ship Techn. Res. 43/1, 1996, pp. 38-47

12. Jensen, G.; Söding, H., "Ship wave-resistance computations", Notes on Num. Fluid Mech. Vol. 25: "Finite approximations in fluid mechanics", Springer, Berlin, Heidelberg, New York, Tokyo, 1989

13. Kajitani, H., "A wandering in some resistance components and flow", Ship Techn. Res. 34/3, 1987, pp. 105-131